minerals

MDPI

Article

Multi-Scale Characterization of Pores and Fractures in Coals with Different Coal-Body Structures from the Jincheng Mine, Qinshui Basin, Northern China

Haoran Yang [1], Xiaomei Wang [1,*], Rui Li [2,*], Pancun Chai [1], Fan Deng [1] and Xingxing Guo [1]

[1] Key Laboratory of Tectonics and Petroleum Resources of Ministry of Education, China University of Geosciences, Wuhan 430074, China; yang_hran@cug.edu.cn (H.Y.); chaipancun@cug.edu.cn (P.C.); 13147198090@163.com (F.D.); 1202110136@cug.edu.cn (X.G.)
[2] School of Resources and Safety Engineering, Chongqing University, Chongqing 400044, China
* Correspondence: xiaomei_wang@cug.edu.cn (X.W.); lirui@cqu.edu.cn (R.L.)

Abstract: The Qinshui Basin is located in the southeast of Shanxi Province, China. It is one of the most abundant coal resources from Permo-Carboniferous North China. It is rich in coal and coalbed methane resources. However, the accumulation of coalbed methane is complex and the enrichment law has not been fully understood because of the high heterogeneity of coal reservoirs in the Qinshui Basin. The examination of dissimilarities between tectonically deformed coals (TDCs) and primary coals at multiple scales holds paramount importance in advancing our understanding of the occurrence and flow patterns of coalbed methane, and in providing guidance for exploration efforts. In the present study, the samples from the Jincheng Mine, Qinshui Basin, were studied by X-ray diffraction (XRD), scanning electron microscopy (SEM), mercury intrusion porosimetry (MIP), CO_2 gas adsorption and 3D X-ray micro-computed tomography. The results showed that the dominant minerals in coal were illite, kaolinite, and calcite, with minor amounts of quartz and ankerite. In comparison to primary coal, tectonism could increase the microfractures density of type A (the fracture of width $\geq$ 5 μm and length > 10 mm) in TDCs. In CO_2 gas adsorption in mylonite coal, it was observed that the volume of micropores (<2 nm) was significantly reduced leading to a decrease in gas adsorption capacity. The result of Micro-CT scanning revealed that the minerals occurred as veins in primary coal, but as irregular aggregates in TDCs. Moreover, tectonism had a staged impact on fracture structure, which was initially closed in cataclastic coal and then formed into granulated coal during the tectonic evolution. The effects of tectonism on coal structure had an impact on the connectivity of micropores at the micrometer scale by the destruction of the pore throat structure, increasing the heterogeneity of the reservoir. These findings help to better understand the changes in TDC structure at different scales for developing effective strategies for coalbed methane exploration and production.

Keywords: TDCs; multi-scale; pore structure; Micro-CT

Citation: Yang, H.; Wang, X.; Li, R.; Chai, P.; Deng, F.; Guo, X. Multi-Scale Characterization of Pores and Fractures in Coals with Different Coal-Body Structures from the Jincheng Mine, Qinshui Basin, Northern China. *Minerals* **2024**, *14*, 833. https://doi.org/10.3390/min14080833

Academic Editors: Samintha Perera and Shifeng Dai

Received: 21 June 2024
Revised: 1 August 2024
Accepted: 12 August 2024
Published: 17 August 2024

1. Introduction

Coal body structure is a foundational factor affecting the physical properties of reservoirs. Coal is highly sensitive to temperature and pressure, leading to deformation and rheology during tectonism [1]. With the development of wrinkling and cracking, tectonically deformed coals (TDCs) such as cataclastic coal, granulitic coal, and mylonite coal [2], are gradually formed [3]. Moreover, TDCs are liable to coal and gas outburst accidents which lead to casualties and economic losses because of their low strength and weakly cohesive morphology compared to primary coal [4–7]. Due to their rather fast initial gas desorption capacity [8], TDC's pore structure properties are crucial factors in gas outburst accidents. The International Union of Pure and Applied Chemistry [9] has published a classification of pores, including micropore, mesopore, and macropore, which have a pore internal width of

<2, 2–50, and >50 nm, respectively [10]. Currently, research methods for the characterization of pore and fracture systems in TDCs could be classified as microscopic imaging methods, measurement methods, and non-intrusive physical methods. Microscopic imaging methods refer to observing microscopic deformation [11,12] to analyze and study the types and deformation characteristics of TDCs using transmission electron microscopy (TEM) [13,14], atomic force microscopy (AFM) [15], and SEM (FIB-SEM/BIB-SEM) [16]. These analytical methods are primarily used to characterize the multi-scale visible microstructure in coal such as distribution and development of pores, fractures, minerals, and other microscopic deformations. However, the limitation of the above methods is the lack of quantitative characterization and a visible holistic distribution of pore–fracture structure. Measurement methods mainly include mercury intrusion porosimetry (MIP) [16,17] and low-pressure gas adsorption (N_2 and CO_2) [18], via molecular probe or fluid intrusion, to represent the quantitative characterization of pore structure in full-scale. MIP with high-pressure mercury intrusion usually leads to damages on pore channel and volume, which showcases an inability to effectively characterize micropores [19]. Although adsorptions of N_2 and CO_2 are effective and accurate, the results of them still have limitations in visual and intuitive characterization. Non-intrusive physical methods investigate the pore size distribution of mesopore and macropore from the aspects of digitization, visualization, non-destruction, topologization, and quantitation, such as nuclear magnetic resonance (NMR) [20,21], small-angle X-ray scattering [22], and 3D X-ray micro computed tomography (X-CT) [14,23]. High-tech tests generally with high precision are too partial to reflect the overall characteristics, especially in TDCs with complex and diverse microstructures. From the above, a single method is not sufficient to adequately detect the pore–fracture structure because of the large span of distribution [24]. Meanwhile, differences in the coal pore–fracture structure characteristics during tectonic evolution are indispensable in the research of expressing the features of desorption/diffusion and permeability.

The investigations of pore–fracture structure in TDCs were conducted through various experiments. Zhai et al. [25] found that tectonic microstructures are developed well in TDCs with a large percentage of mesopores and macropores. By the MIP, N_2, and CO_2 adsorption methods, Wang et al. [3] concluded that the volume of mesopores and macropores increased, as well as the specific surface area (SSA) and porosity. Pan et al. [22] applied AFM to characterize the TDCs' nanostructures, which showed transitional pores, and the porosity increased because of tectonic evolution. Based on the differences in pore structure between high-rank primary coal and TDCs, Xu et al. [26] discussed the influences of tectonism on pore structure and further analyzed the control mechanisms of pore structures on gas adsorption and seepage. This is particularly important for the exploitation of coalbed methane in Qinshui Basin. Compared with other basins, the coal in the Qinshui Basin has characteristics of high-rank and fragmented deformation, resulting in extremely high heterogeneity [27]. The characteristics of pore and fracture development in high-rank tectonic coal reservoirs are not clear, and the microscopic occurrence law and migration mechanism of coalbed methane are unknown. It is difficult to find out the enrichment law of coalbed methane and the development conditions of the 'desert area' [28]. As the tectonism process has different impacts on the characteristics of pore structure on different scales, a comprehensive analysis is required to examine the composition, mineral distribution, pore structure, and connectivity in different coal body structures of TDCs at a multi-scale. This is of great significance to coalbed methane occurrence, flow patterns, and exploration in Qinshui Basin. In addition, the Qinshui Basin is not only rich in coal and coalbed methane resources, but also a large number of key metals, such as Li and Ge, are enriched in coal [29–32]. Therefore, it is necessary to characterize the multi-scale of coal with different coal structures in Qinshui Basin, which is beneficial to the exploitation and comprehensive utilization of coalbed methane.

This study mainly characterized differences in TDCs (cataclastic coal, granulitic coal, and mylonite coal) by proximate analysis, microfracture analyses, XRD, SEM, mercury intrusion porosimetry (MIP), CO_2 gas adsorption, and Micro-CT at the multi-scale. Based

on the results of qualitative and quantitative analysis, this study provides a comprehensive characterization of the pore and fracture structure features of TDCs across multiple scales. Subsequently, it investigates the impact of tectonism on the capacity for gas adsorption and permeability of high-rank TDCs at the nanometer and micron scales, respectively. The findings of this study are crucial for advancing CBM exploitation and promoting safe mining and production practices.

2. Geological Setting

The Qinshui Basin, located in the southeastern of Shanxi Province, Northern China (Figure 1a), is one of the Mesozoic basins evolved from the Late Paleozoic Northern China Craton Basin [33]. The entire basin is surrounded by the uplifts of Taihang Mountain in the east, Huo Mountain in the west, Wutai Mountain in the north, and Zhongtiao Mountain in the south (Figure 1b) [34].

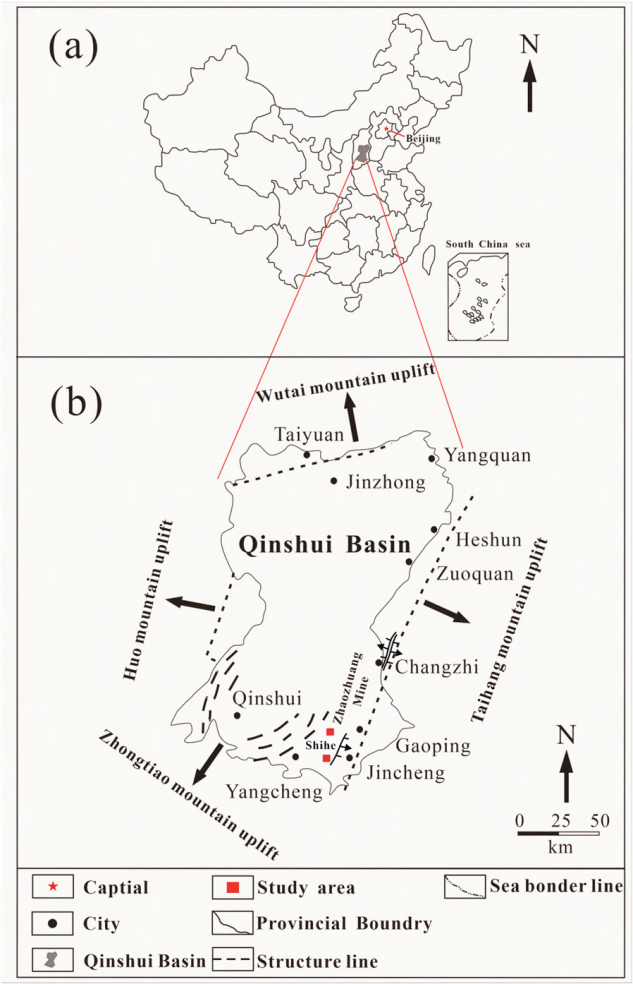

Figure 1. (**a**) Location of the Qinshui Basin in northern China. (**b**) Map of the Qinshui Basin and the location of the study area. Modified from Cai et al. [34].

The Jincheng mining area, located in the west of the southern end of the Taihang Mountain uplift and the southern end of the Qinshui synclinore basin (Figure 1b), is one of the important coal industrial bases in China, and the most favorable region for the commercial development of coalbed methane [35]. In the east of the mining area, the Yihoushan fault, Chengou fault, and Baima fault are distributed in the NNE direction, and in the west of the mining area, the Tuwo-Sitou arc fault is distributed in the NWW-NNE direction. The regional structure of the Jincheng mining area underwent multiple stages of tectonism by the tectonic deformation of Taihang Mountain's orogenic belt after

the coal-bearing formations were formed [26], which deformed the coal and changed the coal properties dramatically, forming TDCs [36]. Although the southern Qinshui Basin has experienced multiple tectonic movements, the deformation of its coal seams is weak. Due to the strong magmatic activity and high degree of coal metamorphism since the Mesozoic era, the coal seams in the southern Qinshui Basin have the characteristics of 'high metamorphism grade and weak deformation'. The strata preserved in Jincheng mining aera include Fengfeng, Benxi, Taiyuan, Shanxi, Xiashihezi, Shangshihezi, Shiqianfeng Formations, and Triassic strata [37]. The coal seams (Figure 2) of the strata in the research area could be high-rank coal because of regional metamorphism. The No. 3 coal seam of the Shanxi Formation and No. 15 coal seam of the Taiyuan Formations are the two main mineable coal seams providing samples [16].

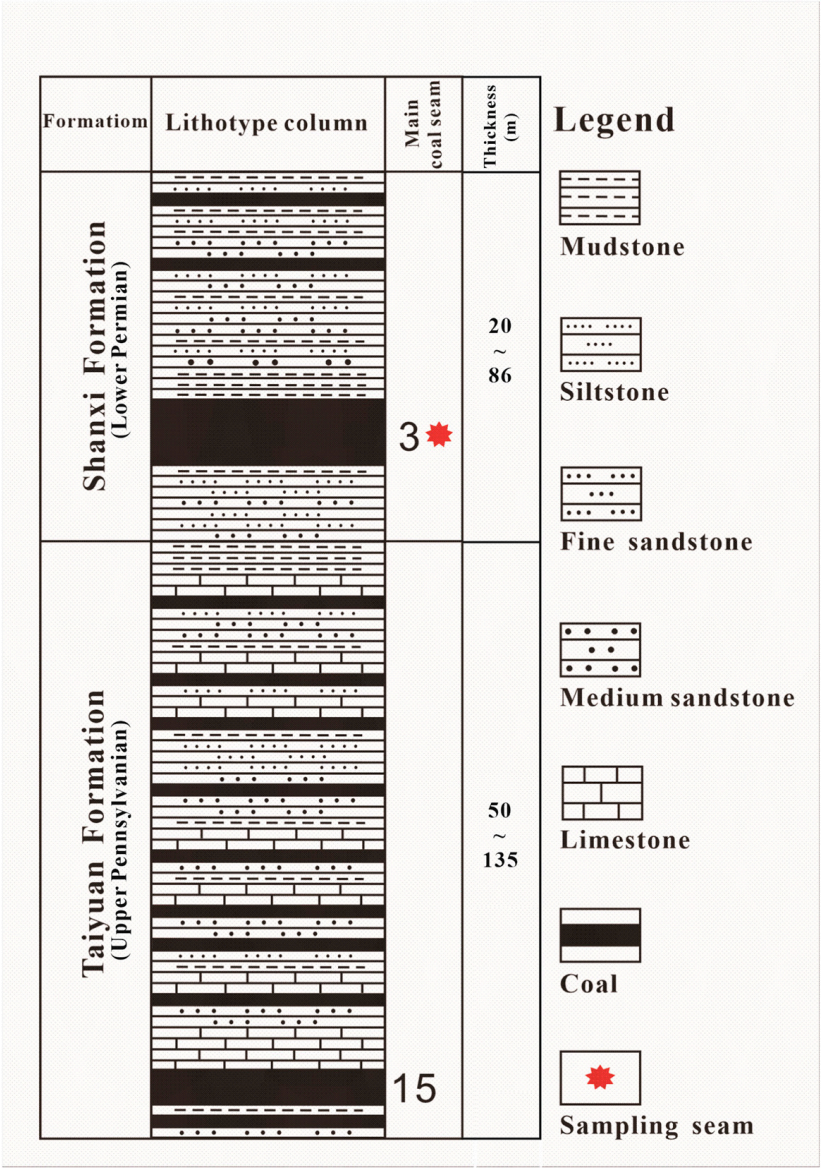

Figure 2. The stratigraphic columns of the Shanxi Formation (sampling seam). Modified from Li et al. [38].

3. Samples and Experiments

3.1. Coal Samples

Samples were collected from the No. 3 coal seam in underground working faces of the Sihe and Zhaozhuang mines. Each bench coal sample of 1–2 kg was collected from

every 20 cm thick coal section. According to the classification scheme of TDCs proposed by Ju et al. [2] concerning the stress–strain environments, four coals were collected from the Jincheng mine areas, classified into 4 classes and shown as Table 1 (primary coal (named as JC-1), cataclastic coal (named as JC-2), granulated coal (named as JC-3), and mylonitic coal (named as JC-4)). These samples were both collected from the No. 3 coal seam of the Shanxi Formation. To prevent these coal samples from further oxidation and eliminate contamination, the samples were stored in sealed plastic bags. The samples were, respectively, crushed to 80 mesh and 200 mesh in agate mortar for proximate analysis, low-pressure gas adsorption analysis, and mineralogical analyses.

Table 1. The contrast of macrocosmic characteristics between samples [2].

Sample No.	Type	Features of Macroscopic Hand Specimens
JC-1	primary coal	With primary structure, having good integrity, and harder to separate.
JC-2	cataclastic coal	Primary structures are still well preserved, accompanied by banded structure. Coal has more than 2 groups of fracture cutting and is hard to separate by hands.
JC-3	granulated coal	The primary structures are destroyed, and stratification is out of order. Coal can be separated into 1–5 cm pieces by hands.
JC-4	mylonitic coal	The primary structures disappear, and crumpled structures widely develop. Coal is easy to be broken into fine grains or powder by hands.

3.2. Analytical Methods

Proximate analysis for coals were conducted following the ASTM D3174–12 [39] for ash, ASTM D3173/D3173M-17a [40] for moisture, and ASTM D3175–17 [41] for fixed carbon and volatile matter. XRD analysis was performed at the State Key Laboratory of Geological Process and Mineral Resources, China University of Geosciences (Wuhan), using an X-ray diffractometer (Panalytical, Malvern, UK, X'Pert Pro, Germany) with Ni-filtered Cu Kα radiation (λ = 0.15418 nm). Each XRD pattern was recorded over a 2θ interval of 3–65°, with a step size of 0.01°. The quantitative mineralogical analysis was conducted by the X'Pert HighScore Plus (3.0.4) instrument software using the K value method, which is an experimental method based on the understanding that there is a positive correlation between the content of a mineral and the intensity of its characteristic diffraction peak.

The morphology and composition of the studied samples were observed by SEM at the State Key Laboratory of Geological Process and Mineral Resources, China University of Geosciences (Wuhan), with a Quanta 200 produced by the FEI Company, The Netherlands. The images can be continuously magnified from five to one million times in intuitive detection, which was provided with a flat fresh section of 1 cm^2 of samples.

The MIP dates were tested in Key Laboratory of Tectonics and Petroleum Resources Ministry of Education, China University of Geoscience (Wuhan), following the ISO 15901-1:2016 standard procedure, using an AutoPore IV 9500 instrument (Micrometrics, Atlanta, GA, USA). Before MIP analysis, all samples were cut into 1 cm^3 and then dried at 105 °C to constant weight. The highest injection pressure in the experiment was 400 MPa, which corresponded to a pore size of about 3 nm, and the maximum pore size measured was about 36 μm.

The low-pressure gas (CO_2) adsorption analysis was tested using a Micromeritics ASAP 2020 surface area and porosity analyzer. All samples were crushed to 80 mesh and degassed under vacuum at 110 °C for 6 h to remove adsorbed volatile substances like moisture or other impurities. The testing pores mainly ranged under 1 nm.

The coal samples were drilled perpendicular to the bedding plane of the coal to obtain a cylindrical core of about 5 mm in diameter and 15 mm in length for a high-resolution helical micro-computed tomography (Micro-CT) scan. The scan was performed on a Skyscan1172 from Bruker company (Germany) with the following parameters: X-ray source, 20–100 kV;

power, 10 W; X-ray detector, 11 Mp or 1.3 Mp Fiber optic taper-coupled CCD camera; detection capability, <1 μm. In this paper, the image pixel is 1.97 μm.

4. Results and Discussions

4.1. Characteristics of Coal Petrography and Coal Quality

The proximate analyses and XRD results of the three different classifications of tectonically deformed coal samples were shown in Table 2. According to the classification of coals (ISO 11760:2018 [42]), the very low-, low-, medium-, moderately high-, and high-ash coals have <5%, 5%–10%, 10%–20%, 20%–30%, and 30%–50% ash yields, respectively. Therefore, the ash yield ranging from 11.128% to 26.612% belonged to medium- to moderately high-ash coals. In addition, the volatile matter content was at a low level (7.105%–11.975%). Obviously in Table 2, the increase in vitrinite reflectance (R_o) investigated that dynamic metamorphism promoted the degree of coalification [43].

Table 2. Proximate analysis (%) and mean random reflectance of vitrinite (Rr, %) in the coal seams.

Sample No.	Rr	Coal Lithotype	Proximate Analysis		
			M_{ad}	A_d	V_{daf}
JC-1	2.67	semi-dull	2.696	26.612	11.975
JC-2	2.92	semi-dull	3.444	14.427	8.203
JC-3	3.60	semi-dull	3.353	11.128	7.105

XRD results in Table 3 showed that the main minerals in the primary coal sample were illite (9.31%) and kaolinite (5.32%), followed by calcite (1.33%) and quartz (2.12%). Additionally, small amounts of chlorite could be observed under SEM. The minerals in the cataclastic coal were mainly calcite (1.44%), illite (10%), kaolinite (1.15%), and ankerite (1.15%). The main minerals in the granulated coal were illite and kaolinite, which accounted for 1.67% and 2.23%, respectively, accompanied by a small amount of iron dolomite (only 0.23%).

Table 3. Mineral compositions (whole coal basis, %) of coal.

Sample No.	Illite	Kaolinite	Quartz	Calcite	Ankerite
JC-1	9.31	5.32	2.12	1.33	-
JC-2	1.44	1.15	-	2.45	1.15
JC-3	1.67	2.23	-	-	0.23

4.2. Characteristics of Pore–Fracture Structures

4.2.1. Characteristics of Microfractures

According to the classification method proposed by Liu et al. [44], microfractures of coal were classified into four types based on its width, length, and continuity observed by optical microscopy [45], including type A (width $\geq$ 5 μm, length > 10 mm), type B (width $\geq$ 5 μm, 1 mm < length $\leq$ 10 mm), type C (width < 5 μm, 300 μm < length $\leq$ 1 mm), and type D (width < 5 μm, length $\leq$ 300 μm). In this study, the density of microfractures (microfracture quantity per 9 cm^2 [46]) was observed and counted via optical microscope.

The predominant type of microfractures in three coals was found to be type B, as shown in Table 4, with densities of 46, 26, and 35 per 9 cm^2, respectively. The length of type B fractures was shorter in primary coal, ranging from 2–5 mm as shown in Figure 3, whereas cataclastic coal and granulated coal had a wider range of fracture lengths, spanning from 1 to 10 mm as depicted in Figure 3. Type A fractures were relatively less abundant, but exhibited an increasing trend in JC-1, JC-2, and JC-3, with densities of 1, 3, and 8 per 9 cm^2, respectively. Type C fractures showed a decreasing trend, as detailed in Table 4. Notably, the fracture structure of mylonite coal was severely fragmented into powder with precluding observations but was tested with adsorption experiments. Overall, the

microfracture density of primary coals is more than that of TDCs, and tectonism could increase the density of type A significantly.

Table 4. Types and densities of the microfractures.

Sample	Microfractures Density (/9 cm^2)				
	Type A	Type B	Type C	Type D	Total
JC-1	1	37	15	6	59
JC-2	3	24	12	7	46
JC-3	8	35	9	6	58

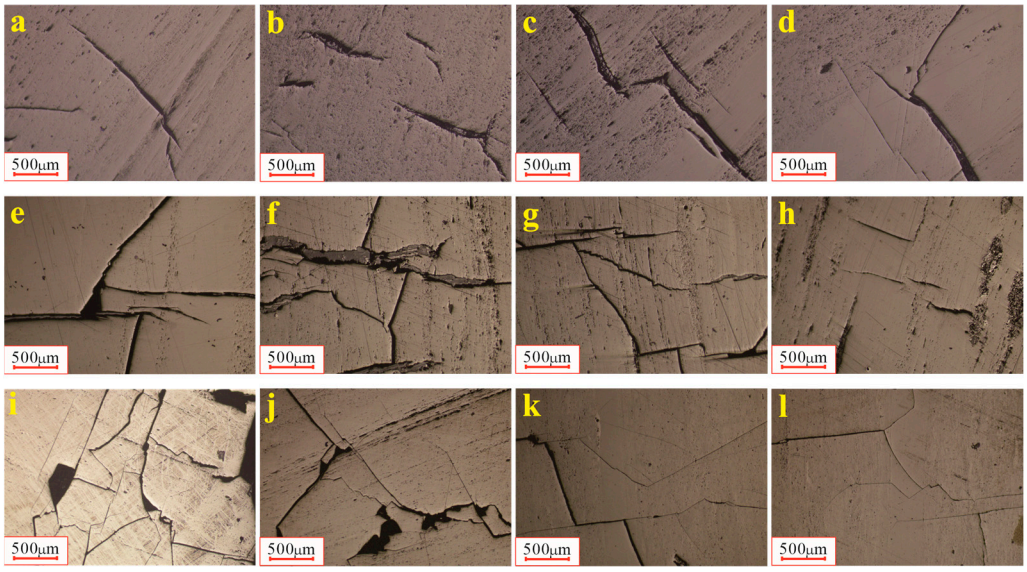

Figure 3. The characteristics of microfractures. (**a**–**d**) JC-1, the characteristics of microfractures, electronic microscope; (**e**–**h**) JC-2, the characteristics of microfractures, electronic microscope; (**i**–**l**) JC-3, the characteristics of microfractures, electronic microscope.

4.2.2. Characteristics of the SEM Pore–Fractures System

Under the SEM scale, the kaolinite mainly occurred as a fracture-filling (Figure 4a–c,f,j), such as filling fractures alone (Figure 4a) or co-existing with chamosite (Figure 4b,c), boehmite (Figure 4j), and calcite (Figure 4f), which indicated the formation of minerals was controlled by different stages of alternating fluid precipitation. In addition, a portion of kaolinite was distributed along the bedding planes (Figure 4a,f). However, the illite occurring as fracture-fillings and ankerite occurring as pore-fillings (Figure 4l) both suggested epigenetic formations (Figure 4h), although, below the detection limit of XRD, some minerals were detected via SEM. For example, albite occurred as individual particles and barite occurred as fine particles aggregates (Figure 4k).

The results of the optical microscope and SEM scales showed that the coal-body structure was conserved well in primary coal, while the brittle fractures took up the main part of TDCs. In the primary coal, the density of microfractures (type A) was lower than TDCs with small fracture apertures (Figure 4a). In addition, the tension joint surface was rough (Figure 4a,b) but the shear joint surface existed smoothly (Figure 4d). However, there were brittle fractures and ductile shear fractures with many secondary associated fractures developing well in TDCs (Figure 4f–i). The coal structure had been severely damaged by tectonism, even presenting irregular granular, scaly, or muddy shapes with minerals (Figure 4k,l).

With a smaller amplification factor, the distribution of minerals in coal could be observed clearly. The minerals in primary coal mainly occurred as fracture-fillings (Figure 5a) and were distributed along the bedding planes in thin layers (Figure 5a,b). Additionally,

the fractures were characterized by long lengths and fewer bifurcations. It also could be observed that some minerals occurred as pore-fillings (Figure 5d). Furthermore, the minerals in granulated coal were scattered in small clumps along the bedding planes or occurred as fracture-fillings (Figure 5e), and paragenesis developed well, which segregated coal structure into different-sized pieces (Figure 5f).

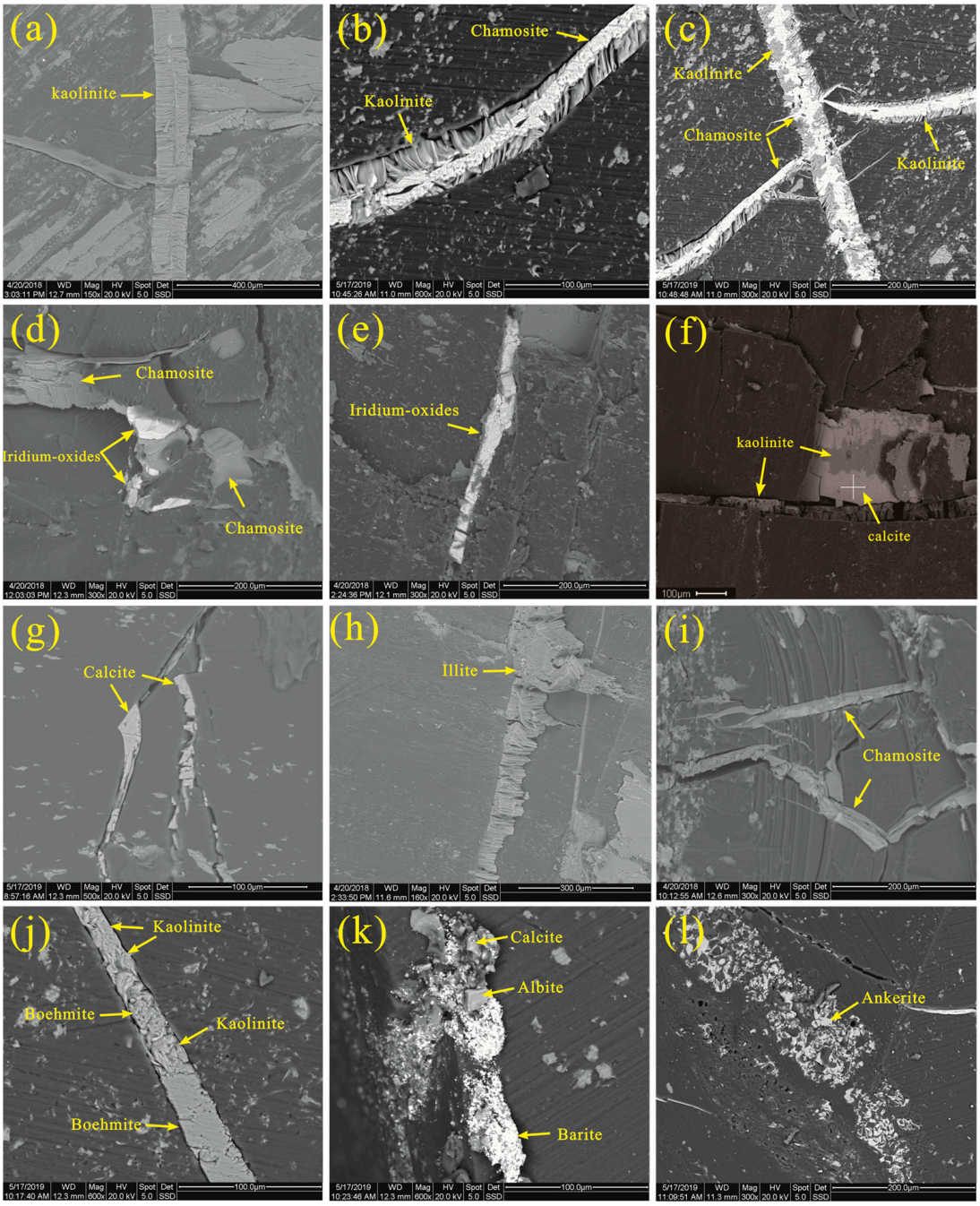

Figure 4. The SEM back-scattered electron images of minerals in sample JC-1, JC-2, and JC-3. (**a**) Kaolinite fills the fracture, sample JC-1. (**b**,**c**) Kaolinite and chamosite paragenesis in fracture, sample JC-1. (**d**) Iridium-oxides and chamosite in sample JC-2. (**e**) Iridium-oxides in sample JC-2. (**f**) Paragenesis of kaolinite and calcite in sample JC-2. (**g**) Calcite fills the fracture, sample JC-2. (**h**) Illite in sample JC-2. (**i**) Chamosite fills the fracture, sample JC-3. (**j**) Kaolinite and boehmite paragenesis in fracture, sample JC-3. (**k**) Barite, albite, and calcite in sample JC-3. (**l**) Ankerite in sample JC-3.

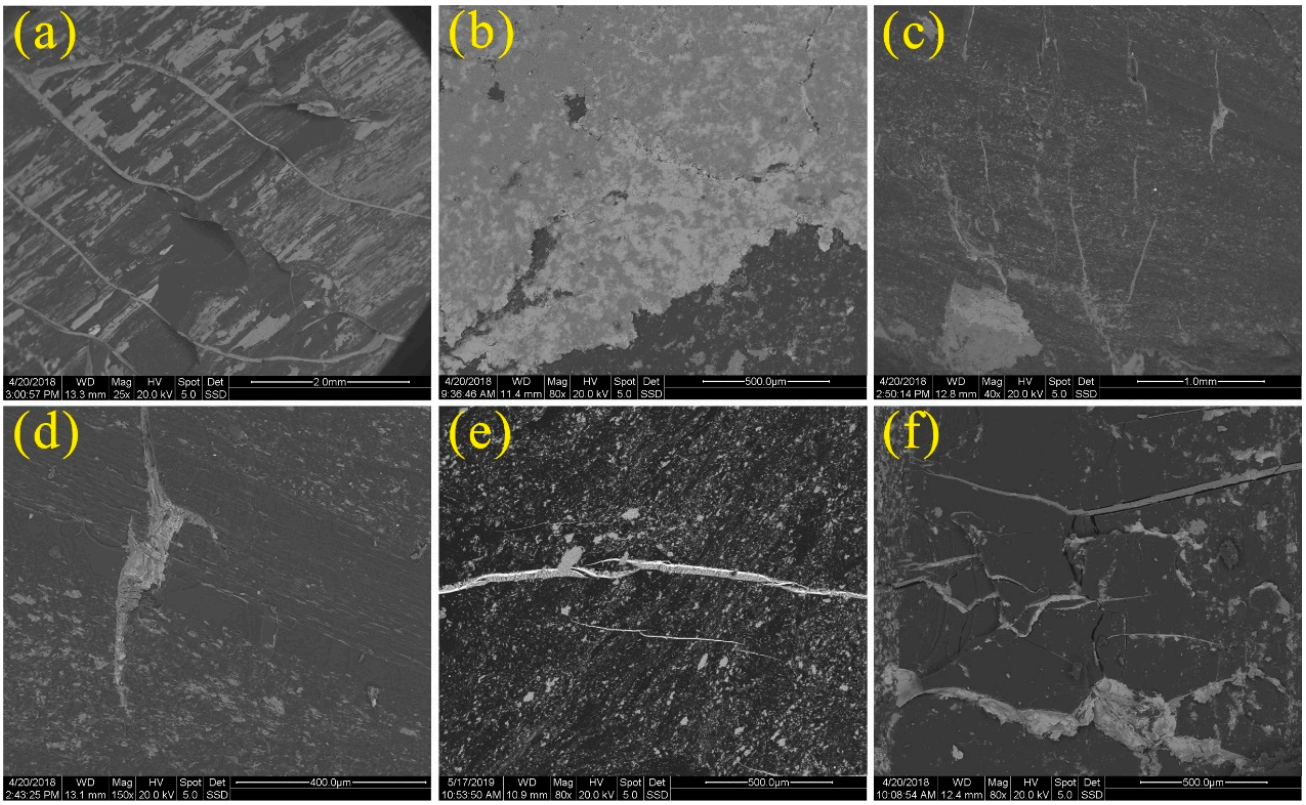

Figure 5. The distribution and the occurrence mode of minerals in primary coal (**a**,**b**), cataclastic coal (**c**,**d**), and granulated coal (**e**,**f**).

4.2.3. Characteristics of Adsorption Pore Structure

The CO_2 adsorption isotherms of samples are displayed in Figure 6. According to the classification of adsorption isotherms by IUPAC, these isotherms were all concave to the p/p° axis belonging to type I, which is usually given to microporous solids with small surface areas.

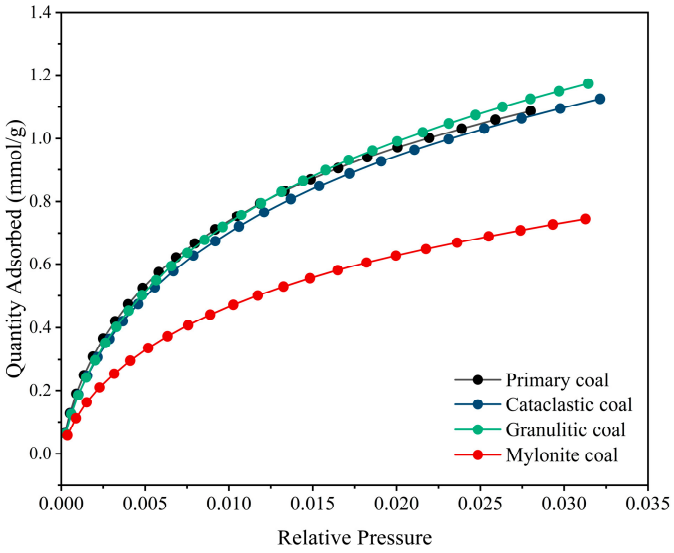

Figure 6. CO_2 gas adsorption isotherms of tectonic coal samples.

The micropore size distributions, incremental volume, and incremental surface area versus pore size of the tectonic coal samples obtained from the CO_2 adsorption experiment are shown in Figure 7. As shown, the pore diameter of all samples was between near 0.40 and 0.90 nm, and the pore diameters between 0.48–0.62 nm and 0.8–0.9 nm were the main distribution area of pore volume and specific surface area with two significant peaks. In addition, the mylonite coal had two similar peaks between 0.48 and 0.62 nm, while in Figure 7b, the incremental surface area with the second peak showed a downward trend compared to the first peak at 0.50–0.60 nm. The phenomenon showed that tectonic deformation caused an increase in complexity [47], which suggested that the high temperature from the tectonic deformation made some micropores collapse, resulting in a decrease in specific surface area. At the same time, the volume of mylonite coal was lower than that of other samples, suggesting that a higher degree of tectonic deformation led to a significant reduction in micropores [18].

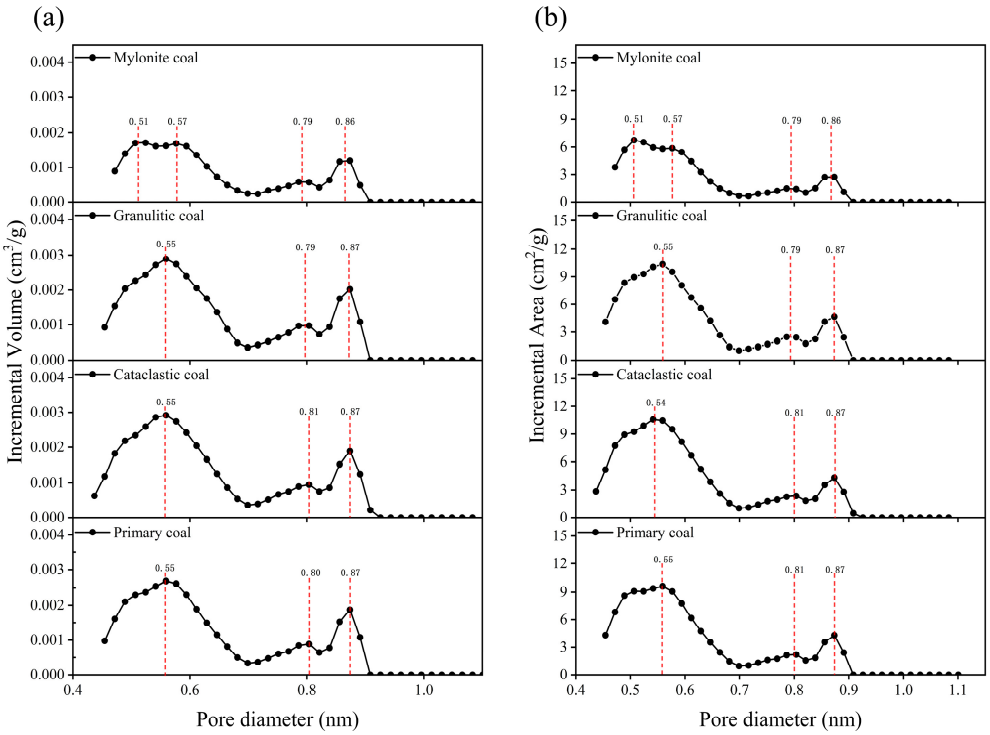

Figure 7. (**a**) Plots of incremental pore volume with respect to the pore diameter; (**b**) plots of incremental surface area with respect to the pore diameter.

4.2.4. Characteristics of the Mercury Intrusion Porosimetry

Figure 8 showed the mercury intrusion–extrusion curves for primary coal, cataclastic coal, granulitic coal, and mylonite coal. At the low-pressure stages, initial points of mercury intrusion are primarily due to macroscopic fractures between particles, which result from the coal sample or the sample preparation process [48,49]. These low-pressure points are usually disregarded in the study of pore fractures in coal. The mercury intrusion–extrusion curves for primary coal and brittle TDCs belonged to the parallel type [50], and their low-pressure mercury intrusion was minimal. At pressures above 10,000 psia, mercury intrusion increased significantly, and the withdrawal efficiency was high. In contrast, the mercury intrusion–extrusion curve for mylonitic coal had a pronounced change, belonging to the double S-type curve with a noticeable 'hysteresis loop'. The mercury withdrawal efficiency was also lower due to the abnormal development of pores.

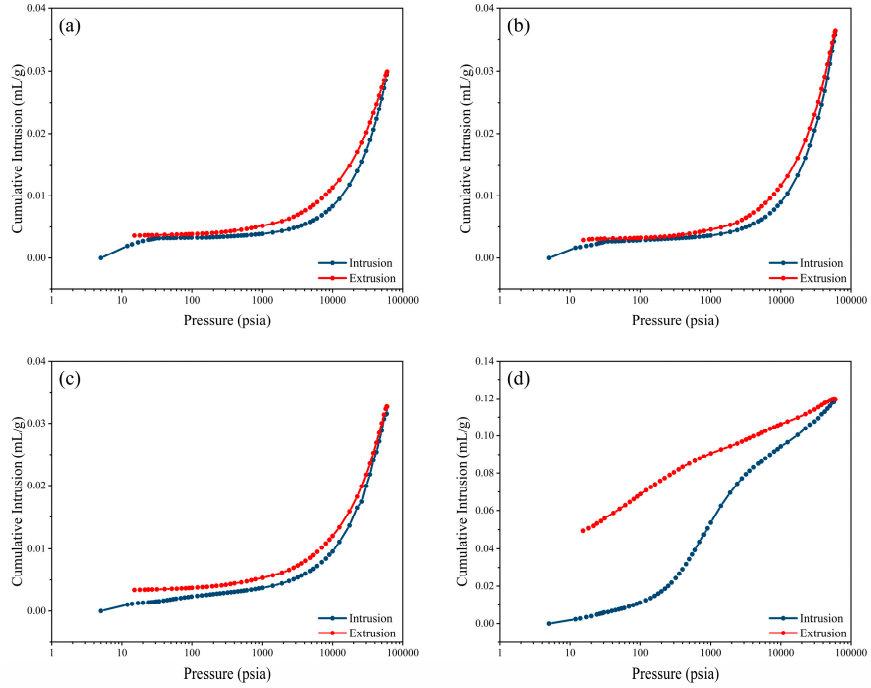

Figure 8. Mercury intrusion and extrusion curves in primary coals and TDCs. Primary coal (**a**), cataclastic coal (**b**), granulitic coal (**c**), and mylonite coal (**d**).

According to the IUPAC classification, the pore diameter distributions are listed in part of Table 5, and the incremental intrusion-pore size curves are shown in Figure 9. The mercury intrusion porosimetry mainly analyzed the pore characteristics of the mesopore and macropore stage of the coal samples. As shown in Figure 9, the pore volume of primary coal, cataclastic coal, and granulated coal generally increased with the decrease in pore diameter and reached their peak at about 10 nm, as well as their pore-specific surface distribution. However, the mylonite coal had many more macropores than other samples and reach its peak at about 100 nm.

Table 5. Characteristics of pore structure of samples in full scale.

Sample	V_z/ ($cm^3 \cdot g^{-1}$)	Stage Pore Capacity/ ($cm^3 \cdot g^{-1}$)			Stage Pore Capacity Ratio/%			S_z/ ($cm^2 \cdot g^{-1}$)	Stage Pore-Specific Surface Area/($cm^3 \cdot g^{-1}$)			Stage Pore-Specific Surface Area Ratio/($cm^3 \cdot g^{-1}$)		
		V_1	V_2	V_3	V_1	V_2	V_3		S_1	S_2	S_3	S_1	S_2	S_3
JC-1	0.0700	0.0405	0.0247	0.0052	57.30	35.30	7.40	146.3770	129.3522	16.9490	0.0750	88.35	11.60	0.05
JC-2	0.0720	0.0393	0.0269	0.006	54.58	37.36	8.06	141.0817	123.0827	17.8854	0.1136	87.24	12.68	0.08
JC-3	0.0740	0.0374	0.0311	0.005	50.45	42.03	7.52	138.2814	116.8182	21.3750	0.0882	84.48	15.46	0.06
JC-4	0.1141	0.0247	0.0382	0.0812	7.18	21.65	71.17	99.0729	74.8070	18.6496	1.6163	75.51	18.82	5.67

Note: IUPAC classification scheme was adopted, V_z and S_z represent the total volume and total specific surface area, respectively; V_1 is the pore volume with D < 2 nm, V_2 is the pore volume with 2 nm < D < 50 nm, and V_3 is the pore volume with D > 50 nm; S_1 is the pore-specific surface area with D < 2 nm, S_2 is the pore-specific surface area with 2 nm < D < 50 nm, S_3 is the pore-specific surface area with D > 50 nm.

The results from the CO_2 gas adsorption and mercury intrusion porosimetry (MIP), as shown in Table 5, revealed the pore structure characteristics of the samples investigated at a full scale. With increasing tectonic degree, the micropore volume of primary coal, cataclastic coal, and granulitic coal decreased slightly but remained over 50%. Conversely, mylonite coal contained only 7.18% micropores and 71.17% macropores, indicating a threshold between granulated and mylonite coal. Beyond this threshold, the micropore volume dropped dramatically, while the mesopore and macropore volumes increased, constituting a significant proportion of the pore structure in mylonite coal.

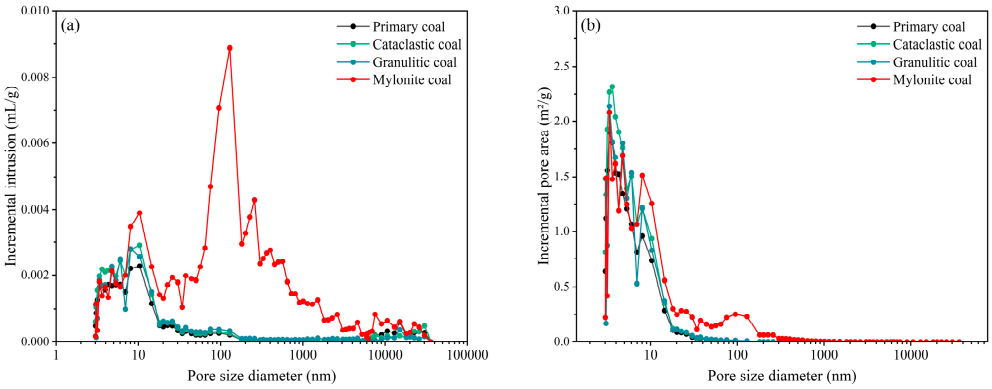

Figure 9. Pore volume distribution and pore-specific surface area based on MIP. ((**a**) is the relationship between pore diameter and pore volume on coal samples, (**b**) is the relationship between pore diameter and pore area on coal samples).

4.2.5. Characteristics of Micro-CT Scanning and 3D Reconstruction

Micro-CT results produced 8-bit 2D images with gray-scale values ranging from 0 to 255. The gray-scale values differed due to the varying densities of different components of the coal. Higher densities corresponded to higher gray-scale values. Consequently, fractures and pores appeared black in CT images, while minerals appeared light white. The gray-scale value of minerals ranged from 150 to 255, while the gray-scale value of pores and fractures ranged from 0 to 50. The gray-scale value of organic matter in coal fell between the gray-scale values of minerals and pores. After determining the gray-scale values, the CT scan data were reconstructed using Avizo 2019. As shown in Figure 10, the minerals occurred as veins in primary coal which had a complete fracture structure. However, as the degree of tectonic deformation increased, the fracture structure gradually deteriorated, and minerals transformed into irregular aggregates. Furthermore, based on the SEM results, it could be inferred that minerals were predominantly present in fractures in the primary coal. Under long-term tectonic stress, primary coal evolved into the tectonic coal with the content of fractures and pores increasing, becoming strongly extruded, sheared, and deformed [51,52]. Therefore, mineral layers in coal were gradually extruded into patchy and irregular granules.

After reconstructing a 3D model of the samples, the pores and fractures were extracted by Avizo as shown in Figure 11d–f. The following could be seen as the process of fracture evolution in tectonic deformation: Figure 11d,e, the fractures closing stage; and Figure 11e,f, the microfractures development stage [46]. In the process of brittle deformation, two stages corresponded to different coal structures and unique physical characteristics. In the evolution from primary coal to cataclastic coal, fractures closed under pressure, leading to lower permeability. According to the calculation module of permeability in Avizo, permeability changed from 0.00304 mD of primary coal to 0.00117 mD of cataclastic coal. Then, with the increase in stress, some microfractures are formed. This corresponded to the evolution process from cataclastic coal to granulated coal. The permeability also increased slightly to 0.00238 mD.

Figure 12 shows the distribution of the pores' radii, which presents that the proportion of pores (radius > 10 μm) increases with the tectonic process, and the volume contribution of pores (radius > 10 μm) in tectonic coal is also more than primary. Meanwhile, the connected pores were extracted by Avizo, as shown in Figure 13. The pore network was modeled based on the tagged interconnected pores. In this model, the interconnected pore clusters replaced by spheres of equivalent radius, connected through the throat of equivalent radius. Compared with TDCs, the pore throat structure of primary coal was more complete, and the development of pores and throats was more balanced. The distribution of interconnected pores in TDCs (Figure 13b,c) was stratified, and the throats of the TDCs were more cluttered with narrow radii.

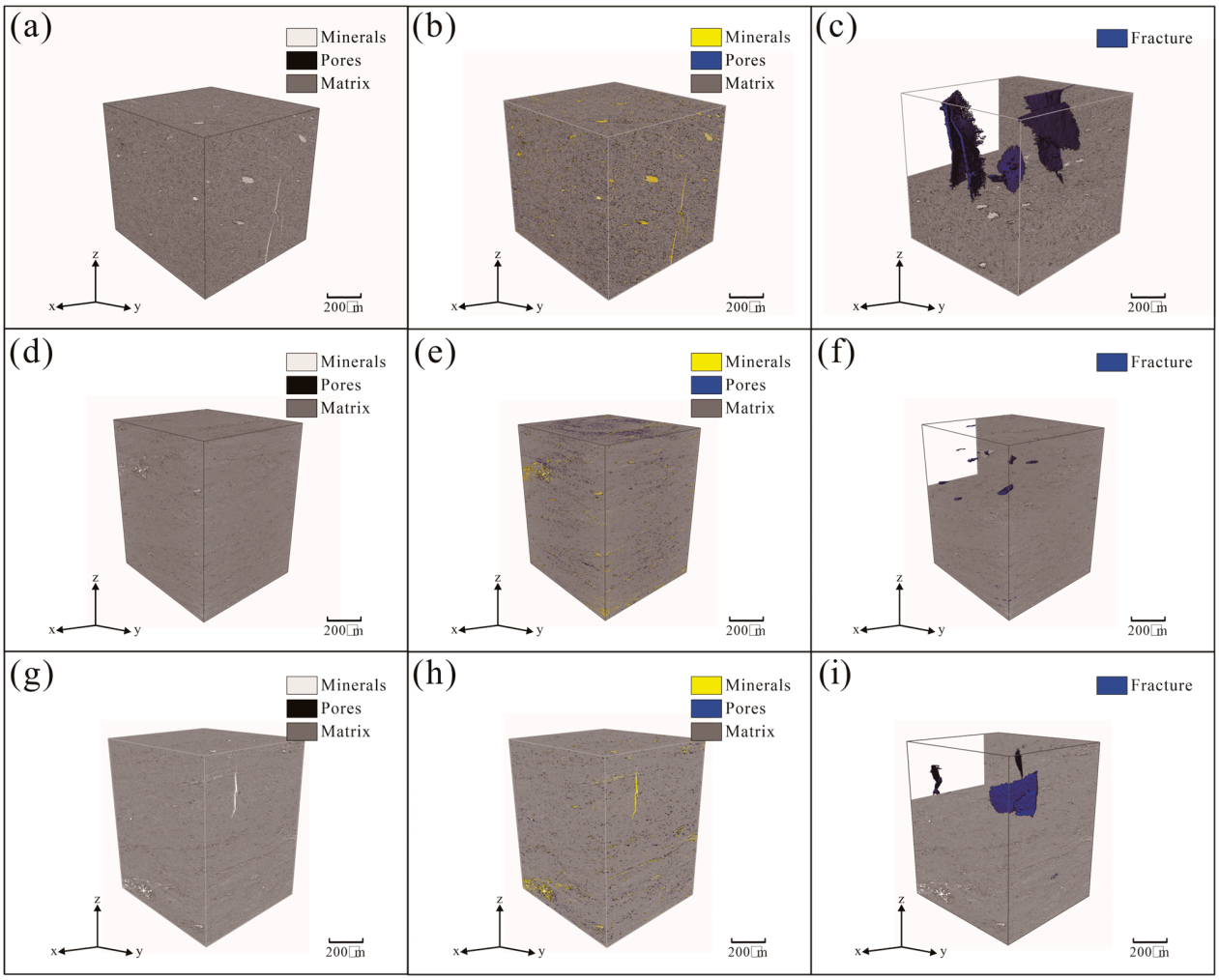

Figure 10. Reconstructed 3D model of samples, JC-1 (**a**–**c**), JC-2 (**d**–**f**), and JC-3 (**g**–**i**).

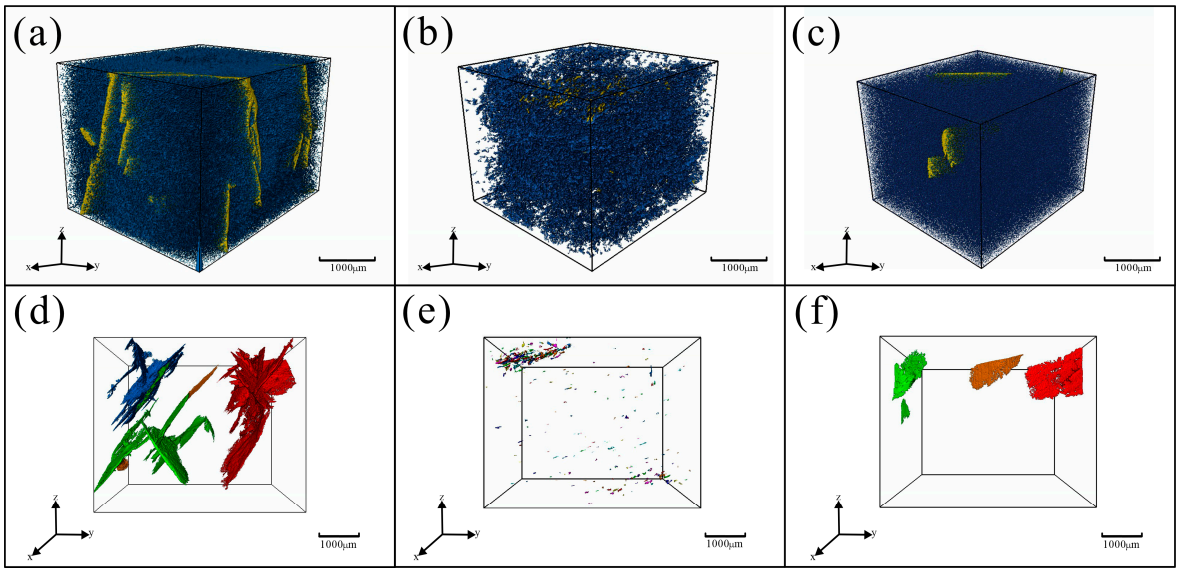

Figure 11. Three-dimensional visualization of the pores and fractures (Blue shading indicates the pores and yellow shading indicates the fractures in (**a**–**c**), different-colored shadings indicate different fractures in (**d**–**f**)).

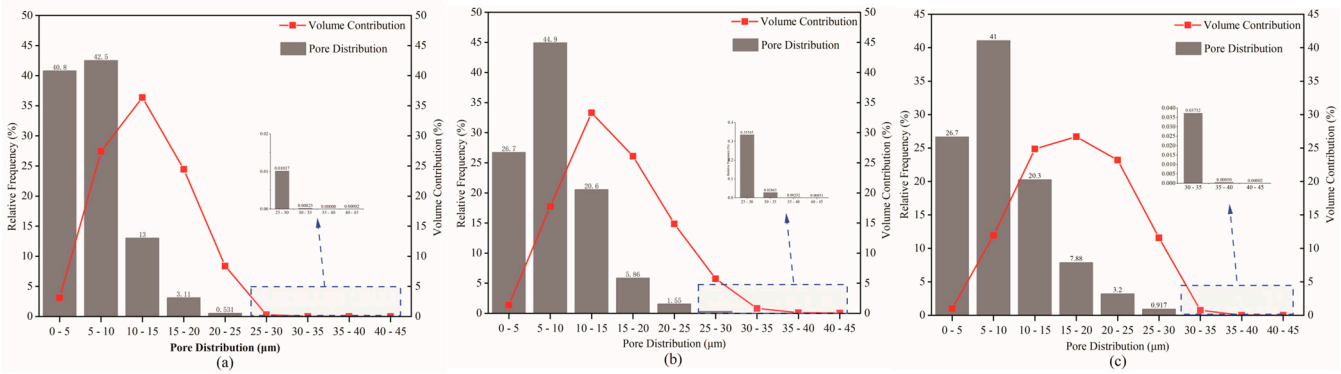

Figure 12. Distribution frequency of pore radius, JC-1 (**a**), JC-2 (**b**), and JC-3 (**c**).

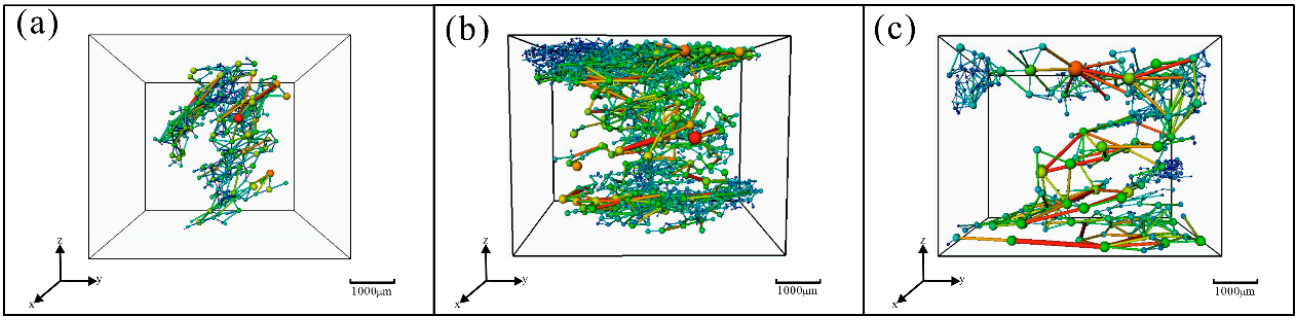

Figure 13. The model of interconnected porosity and pore network (JC-1 (**a**), JC-2 (**b**), and JC-3 (**c**)), the warmer the color of the pores and throats, the larger the diameter.

Quantitative analysis of interconnected pores and throats is presented in Figures 14 and 15. In general, the tectonic deformation made the main proportion of coordination number transfer to larger. This meant that the number of connections between pores became more. However, the throats of connecting pores were also an important factor. From Figure 15, most throats in cataclastic coal were narrow, which had a less effective volume contribution. It led to a lower permeability of cataclastic coal.

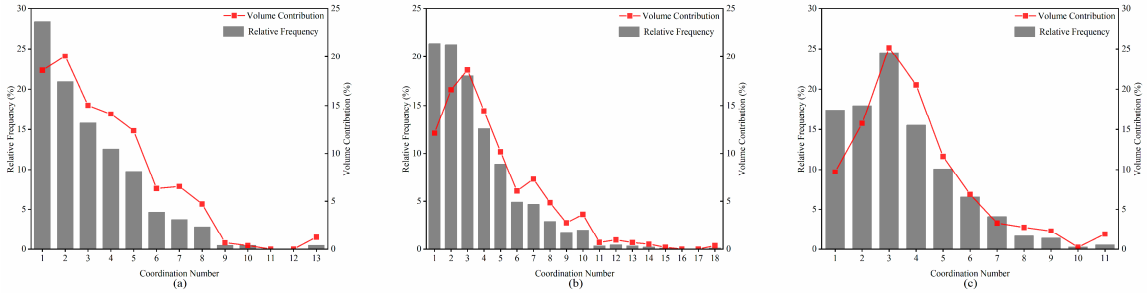

Figure 14. Distribution frequency of the coordination numbers, and the volume contrbuition of the coordination numbers (**a**–**c**).

On different scales, there were remarkable changes in pore structure between TDCs and primary coal. CO_2 adsorption and MIP methods, connected in Table 5, revealed that the volume of micropores decreases, and mesopores and macropores increases during the tectonic evolution. In the present study, mylonite coal had a reduction in the volume of micropores, suggesting that a higher degree of tectonic deformation may lead to the reduction in the amount of micropores [18]. However, the tectonic deformation promoted the development of mesopores and macropores [26,53]. As shown in Table 5, V_1 (volume of micropore) had an overall light decrease with the higher degree of tectonic deformation, but

V_1 reduced sharply in mylonite coal. With the increase in the level of tectonic deformation, V_2 (volume of mesopore) increased except for the reduced proportion of V_2 in mylonite coal. These phenomena revealed that with the enhancement of structural deformation, the macromolecular structure of coal increased, forming mesopores between aromatic nuclei and aromatic layers. Additionally, it was a remarkable increase that the V_3 (volume of macropore) had in mylonite coal because of strong tectonic deformation. The development of breccia pores, granular pores, and friction pores resulting from tectonic deformation was promoted by structural deformation and mutual friction. Compared to previous findings, the results regarding micropore volume were partly inconsistent with Li et al.'s [54] observation that tectonic deformation increased the volume of micropores, while being consistent with the decline in the percentage of micropores. The reason could be the different degrees of impact of various tectonic processes on the pore structure, and the decrease in micropore volume may be due to the shear tectonic deformation. Li [50] classified various types of tectonic deformation in TDCs as cataclastic deformation, shear deformation, granular deformation, crumpled deformation, and composite deformation. When TDCs underwent shear deformation, it significantly decreased the volume of micropores due to the destruction of the primary micropores of the coal body and promoted the development of macrofractures. The strong shear tectonic deformation led to the fragmentation and pulverization of coal, resulting in the collapse of some micropores. Then, these micropores were interconnected under the action of stress, forming mesopores. In reconstructing a 3D model of the samples, tectonic deformation changed the μm-scale structure of the coal. It revealed that the fractures are closed first in cataclastic coal and then formed in granulated coal during the process of tectonic evolution. According to the distribution of pores and throats, tectonic deformation increased the heterogeneity of coal, destroyed the original seepage path, and reduced the permeability of tectonic coal. The extremely strong heterogeneity leads to the phenomenon of low selection accuracy of favorable blocks for coalbed methane and poor applicability of reservoir reconstruction technology.

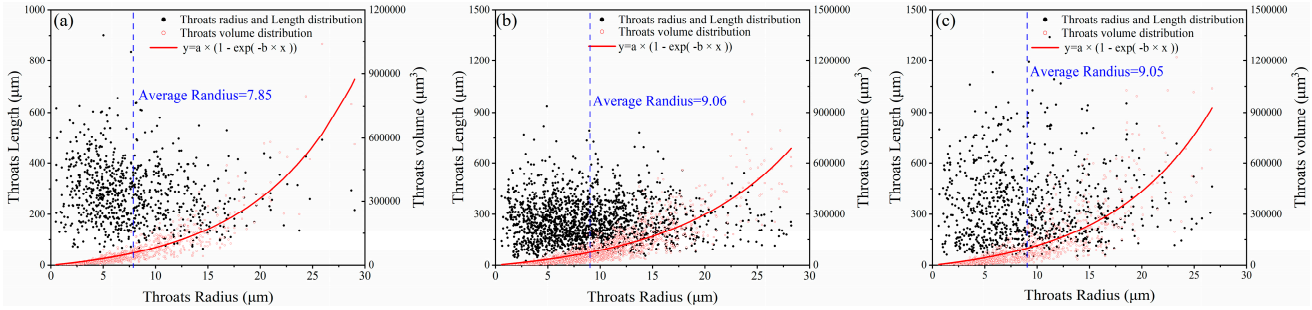

Figure 15. Distribution of pore throat radius, pore throat length, and cumulative volume contribution relationship (**a**–**c**).

5. Conclusions

The development of multiscale porosity between the primary coal and TDCs was studied by microscopic observation, SEM, adsorption of CO_2, MIP, and Micro-CT scanning. The following conclusions were reached:

(1) The coal from the Jincheng mine was classified as low- to medium-ash coals and low volatile bituminous coal. The minerals in the coal matrix predominantly consisted of illite, kaolinite, and calcite, with a small amount of quartz and ankerite. It was speculated that tectonism may have played a role in the elevation of coal rank.

(2) The microfractures from microscopic observation were dominated by type B, and the number of type B in cataclastic coal was the least among the other samples. The density of type A fractures significantly increased with tectonic deformation. These results were consistent with the observations at the micron scale, where the fracture structure of the coal underwent gradual changes with tectonism. A 3D model of the CT images demonstrated that the fractures in cataclastic coal tended to close under the

influence of tectonism, while the granulated coal exhibited an increase in the number of fractures with the increase in tectonic deformation.

(3) During the process of tectonic deformation, tectonism resulted in the degradation of the structural integrity of coal and an increase in pore content. According to the SEM scale, the minerals in primary coal mainly filled fractures appearing veiny, partially in flakes or irregular granules. Conversely, in cataclastic and granulated coals, the minerals appeared as irregular granules and aggregates filling the pores.

(4) It was found that the effect of tectonic deformation on micropores (<2 nm) was not significant, especially in weakly deformed coals such as cataclastic coal and granulated coal, while the micropore volume of mylonite coal had a decrease. This showed that different levels of tectonism had different effects on micropore structure. The decrease in micropore volume may be due to the shear tectonic deformation.

(5) A 3D model of the CT images showed that minerals existed in irregular aggregates in tectonic coal. In comparing primary coal to TDCs, the latter had a larger pore radius at the μm scale, yet had lower permeability. The rationale for this phenomenon was that the tectonic deformation had significantly destroyed the primary coal's structure, leading to more complex and shorter throats of the interconnected pores.

Author Contributions: Conceptualization: H.Y., X.W. and R.L.; methodology: H.Y., P.C., F.D. and X.G.; formal analysis and investigation: H.Y. and P.C.; writing—original draft preparation: H.Y.; writing—review and editing: H.Y., X.W. and R.L.; resources: R.L. All authors have read and agreed to the published version of the manuscript.

Funding: This research was financially supported by the National Natural Science Foundation of China (Nos. 42372190, 42172194, 41972181, and 52204125), the National Key Research and Development Program of China (No. 2021YFC2902000), and the Major Science and Technology Department Program of Xinjiang Uygur autonomous region (No. 2022A03014-2).

Data Availability Statement: Data is contained within the article.

Acknowledgments: The authors thank the anonymous reviewers for their critical remarks and comments, which greatly helped to improve the manuscript.

Conflicts of Interest: The authors have no relevant financial or non-financial interests to disclose. The authors have no competing interests to declare that are relevant to the content of this article. All authors certify that they have no affiliations with or involvement in any organization or entity with any financial interest or non-financial interest in the subject matter or materials discussed in this manuscript. The authors have no financial or proprietary interests in any material discussed in this article.

References

1. Cao, D.; Li, X.; Deng, J. Coupling Effect Between Coalification and Tectonic-thermal Events-Geological Records of Geodynamics of Sedimentary Basin. *Earth Sci. Front.* **2009**, *16*, 52–60. [CrossRef]
2. Ju, Y.; Jiang, B.; Hou, Q.; Wang, G. The new structure-genetic classification system in tectonically deformed coals and its geological significance. *J. China Coal Soc.* **2004**, *29*, 514–517. (In Chinese)
3. Wang, Z.; Cheng, Y.; Qi, Y.; Wang, R.; Wang, L.; Jiang, J. Experimental study of pore structure and fractal characteristics of pulverized intact coal and tectonic coal by low temperature nitrogen adsorption. *Powder Technol.* **2019**, *350*, 15–25. [CrossRef]
4. Ma, J.; Qi, H.; Wong, P. Experimental study of multilayer adsorption on fractal surfaces in porous media. *Phys. Rev. E* **1999**, *59*, 2049–2059. [CrossRef]
5. Li, H.; Ogawa, Y.; Shimada, S. Mechanism of methane flow through sheared coals and its role on methane recovery. *Fuel* **2003**, *82*, 1271–1279. [CrossRef]
6. Mark, C. Coal bursts that occur during development: A rock mechanics enigma. *Int. J. Min. Sci. Technol.* **2018**, *28*, 35–42. [CrossRef]
7. Geng, J.; Cao, L.; Zhong, C.; Zhang, S. An Experimental Study on Preparation of Reconstituted Tectonic Coal Samples: Optimization of Preparation Conditions. *Energies* **2021**, *14*, 2846. [CrossRef]
8. Tu, Q.; Cheng, Y.; Ren, T.; Wang, Z.; Lin, J.; Lei, Y. Role of Tectonic Coal in Coal and Gas Outburst Behavior During Coal Mining. *Rock Mech. Rock Eng.* **2019**, *52*, 4619–4635. [CrossRef]

9. IUPAC (International Union of Pure and Applied Chemistry). Physical chemistry division commission on colloid and surface chemistry, subcommittee on characterization of porous solids: Recommendations for the characterization of porous solids (Technical report). *Pure Appl. Chem.* **1994**, *8*, 1739–1758.
10. Thommes, M. Physical Adsorption Characterization of Nanoporous Materials. *Chem. Ing. Tech.* **2010**, *82*, 1059–1073. [CrossRef]
11. Li, M.; Jiang, B.; Lin, S.; Wang, J.; Ji, M.; Qu, Z. Tectonically deformed coal types and pore structures in Puhe and Shanchahe coal mines in western Guizhou. *Int. J. Min. Sci. Technol.* **2011**, *21*, 353–357. [CrossRef]
12. Ni, X.; Chen, W.; Li, Z.; Gao, X. Reconstruction of different scales of pore-fractures network of coal reservoir and its permeability prediction with Monte Carlo method. *Int. J. Min. Sci. Technol.* **2017**, *27*, 693–699. [CrossRef]
13. Yao, Y.; Liu, D.; Tang, D.; Tang, S.; Huang, W. Fractal characterization of adsorption-pores of coals from North China: An investigation on CH_4 adsorption capacity of coals. *Int. J. Coal Geol.* **2008**, *73*, 27–42. [CrossRef]
14. Yao, Y.; Liu, D.; Che, Y.; Tang, D.; Tang, S.; Huang, W. Non-destructive characterization of coal samples from China using microfocus X-ray computed tomography. *Int. J. Coal Geol.* **2009**, *80*, 113–123. [CrossRef]
15. Lawrie, G.A.; Gentle, I.R.; Fong, C.; Glikson, M. Atomic force microscopy studies of Bowen Basin coal macerals. *Fuel* **1997**, *76*, 1519–1526. [CrossRef]
16. Liu, S.; Sang, S.; Wang, G.; Ma, J.; Wang, X.; Wang, W.; Du, Y.; Wang, T. FIB-SEM and X-ray CT characterization of interconnected pores in high-rank coal formed from regional metamorphism. *J. Petrol. Sci. Eng.* **2016**, *148*, 21–31. [CrossRef]
17. Okolo, G.N.; Everson, R.C.; Neomagus, H.W.J.P.; Roberts, M.J.; Sakurovs, R. Comparing the porosity and surface areas of coal as measured by gas adsorption, mercury intrusion and SAXS techniques. *Fuel* **2015**, *141*, 293–304. [CrossRef]
18. Hou, S.; Wang, X.; Wang, X.; Yuan, Y.; Pan, S.; Wang, X. Porestructure characterization of low volatile bituminous coals with different particle size and tectonic deformation using low pressure gas adsorption. *Int. J. Coal Geol.* **2017**, *183*, 1–13. [CrossRef]
19. Bustin, R.M.; Bustin, A.M.M.; Cui, A.; Ross, D.; Pathi, V.M. Impact of Shale Properties on Pore Structure and Storage Characteristics. In Proceedings of the SPE Shale Gas Production Conference, Fort Worth, TX, USA, 16–18 November 2008. Paper Number: SPE-119892-MS. [CrossRef]
20. Li, X.; Kang, Y.; Haghighi, M. Investigation of pore size distributions of coals with different structures by nuclear magnetic resonance (NMR) and mercury intrusion porosimetry (MIP). *Measurement* **2018**, *116*, 122–128. [CrossRef]
21. Zhao, Y.; Sun, Y.; Liu, S.; Wang, K.; Jiang, Y. Pore structure characterization of coal by NMR cryoporometry. *Fuel* **2017**, *190*, 359–369. [CrossRef]
22. Pan, J.; Niu, Q.; Wang, K.; Shi, X.; Li, M. The closed pores of tectonically deformed coal studied by small-angle X-ray scattering and liquid nitrogen adsorption. *Microporous Mesoporous Mater.* **2016**, *224*, 245–252. [CrossRef]
23. Zhang, K.; Wang, S.; Wang, L.; Cheng, Y.; Li, W.; Han, X.; Liu, C.; Su, H. 3D visualization of tectonic coal microstructure and quantitative characterization on topological connectivity of pore-fracture networks by Micro-CT. *J. Petrol. Sci. Eng.* **2022**, *208*, 109675. [CrossRef]
24. Zhang, G.; Ranjith, P.G.; Fu, X.; Li, X. Pore-fracture alteration of different rank coals: Implications for CO_2 sequestration in coal. *Fuel* **2021**, *289*, 119801. [CrossRef]
25. Zhai, J.; Wang, J.; Lu, G.; Qin, X.; Wang, W. Permeability characteristics of remolded tectonically deformed coal and its influence factors. *J. Nat. Gas Sci. Eng.* **2018**, *53*, 22–31. [CrossRef]
26. Xu, X.; Meng, Z.; Wang, Y. Experimental comparisons of multiscale pore structures between primary and disturbed coals and their effects on adsorption and seepage of coalbed methane. *J. Petrol. Sci. Eng.* **2019**, *174*, 704–715. [CrossRef]
27. Zhang, Z.; Ren, J.; Zhao, Y.; Wang, M.; Yang, J.; Zhang, C. Geological Characteristics of Low-Yield and Low-Efficiency CBM Wells and Practical Measures for Production Increase in the Qinshui Basin. *ACS Omega* **2023**, *8*, 47530–47539. [CrossRef]
28. Yang, Y.; Wang, Y.; Liu, Z.; Chen, B.; Wu, C.; Zhang, X.; Dong, Q. Strategy and practice of high-efficiency development of high-rank coalbed methane in the southern Qinshui Basin. *China Pet. Explor.* **2024**, *29*, 18–31. (In Chinese) [CrossRef]
29. Zhang, W.; Zhao, L.; Wang, W.; Nechaev, V.P.; French, D.; Graham, I.; Lang, Y.; Li, Z.; Dai, S. Enrichment of critical metals (Li, Ga, and rare earth elements) in the early Permian coal seam from the Jincheng Coalfield, southeastern Qinshui Basin, northern China: With an emphasis on cookeite as the Li host. *Ore Geol. Rev.* **2024**, *167*, 105939. [CrossRef]
30. Hou, Y.; Dai, S.; Nechaev, V.P.; Finkelman, R.B.; Wang, H.; Zhang, S.; Di, S. Mineral matter in the Pennsylvanian coal from the Yangquan Mining District, northeastern Qinshui Basin, China: Enrichment of critical elements and a Se-Mo-Pb-Hg assemblage. *Int. J. Coal Geol.* **2023**, *266*, 104178. [CrossRef]
31. Hou, Y.; Liu, D.; Zhao, F.; Zhang, S.; Zhang, Q.; Emmanuel, N.N.; Zhong, L. Mineralogical and geochemical characteristics of coal from the Southeastern Qinshui Basin: Implications for the enrichment and economic value of Li and REY. *Int. J. Coal Geol.* **2022**, *264*, 104136. [CrossRef]
32. Zhao, L.; Dai, S.; Nechaev, V.P.; Nechaeva, E.V.; Graham, I.T.; French, D. Enrichment origin of critical elements (Li and rare earth elements) and a Mo-U-Se-Re assemblage in Pennsylvanian anthracite from the Jincheng Coalfield, southeastern Qinshui Basin, northern China. *Ore Geol. Rev.* **2019**, *115*, 103184. [CrossRef]
33. Zhang, M.; Fu, X. Characterization of pore structure and its impact on methane adsorption capacity for semi-anthracite in Shizhuangnan Block, Qinshui Basin. *J. Nat. Gas Sci. Eng.* **2018**, *60*, 49–62. [CrossRef]
34. Cai, Y.; Liu, D.; Yao, Y.; Li, J.; Qiu, Y. Geological controls on prediction of coalbed methane of No. 3 coal seam in Southern Qinshui Basin, North China. *Int. J. Coal Geol.* **2011**, *88*, 101–112. [CrossRef]

35. Zhao, L.; Ward, C.R.; French, D.; Graham, I.T.; Dai, S.; Yang, C.; Xie, P.; Zhang, S. Origin of a kaolinite-NH_4-illite-pyrophyllite-chlorite assemblage in a marine-influenced anthracite and associated strata from the Jincheng Coalfield, Qinshui Basin, Northern China. *Int. J. Coal Geol.* **2018**, *185*, 61–78. [CrossRef]
36. Cheng, Y.; Pan, Z. Reservoir properties of Chinese tectonic coal: A review. *Fuel* **2020**, *260*, 116350. [CrossRef]
37. Su, X.; Lin, X.; Liu, S.; Zhao, M.; Song, Y. Geology of coalbed methane reservoirs in the Southeast Qinshui Basin of China. *Int. J. Coal Geol.* **2005**, *62*, 197–210. [CrossRef]
38. Ju, Y.; Jiang, B.; Hou, Q.L.; Tan, Y.; Guiliang, W.; Xiao, W. Behavior and mechanism of the adsorption/desorption of tectonically deformed coals. *Chin. Sci. Bull.* **2009**, *54*, 88–94. [CrossRef]
39. *ASTM Standard D3174-12*; Standard Test Method for Ash in the Analysis Sample of Coal and Coke from Coal. ASTM International: West Conshohocken, PA, USA, 2012.
40. *ASTM Standard D3173/D3173M*; Standard Test Method for Moisture in the Analysis Sample of Coal and Coke. ASTM International: West Conshohocken, PA, USA, 2017.
41. *ASTM Standard D3175-17*; Standard Test Method for Volatile Matter in the Analysis Sample of Coal and Coke. ASTM International: West Conshohocken, PA, USA, 2020.
42. *ISO Standard 11760*; Classification of Coals. International Organization for Standardization: Geneva, Switzerland, 2018.
43. Deng, X.; Hu, Q.; Wei, S. Genesis and Property Classfication of Tectonic Coal. *J. Eng. Geol.* **2014**, *22*, 1008–1014.
44. Liu, D.; Yao, Y.; Tang, D.; Tang, S.; Che, Y.; Huang, W. Coal reservoir characteristics and coalbed methane resource assessment in Huainan and Huaibei coalfields, Southern North China. *Int. J. Coal Geol.* **2009**, *79*, 97–112. [CrossRef]
45. Yao, Y.; Liu, D.; Huang, W.; Tang, D.; Tang, S. Research on the pore-fractures system properties of coalbed methane reservoirs and recovery in Huainan and Huaibei coal-fields. *J. China Coal Soc.* **2006**, *31*, 163–168.
46. Li, S.; Tang, D.; Xu, H.; Yang, Z. Advanced characterization of physical properties of coals with different coal structures by nuclear magnetic resonance and X-ray computed tomography. *Comput Geosci.* **2012**, *48*, 220–227. [CrossRef]
47. Guo, D.; Guo, X.; Li, D. Effects of tectonic deformation on micropore-mesopore of bituminous deformed coal. *J. China Coal Soc.* **2019**, *10*, 3135–3144. [CrossRef]
48. Stanmore, B.R.; He, Y.; White, E.T.; Firth, B.; O'Brien, G.; O'Brien, M. Porosity and water retention in coarse coking coal. *Fuel* **1997**, *76*, 215–222. [CrossRef]
49. Li, Y.; Lu, G.Q.; Rudolph, V. Compressibility and Fractal Dimension of Fine Coal Particles in Relation to Pore Structure Characterisation Using Mercury Porosimetry. *Part. Part. Syst. Charact.* **1999**, *16*, 25–31. [CrossRef]
50. Li, M. Structure Evolution and Deformation Mechanism of Tectonically Deformed Coal. Master's Thesis, China University of Mining and Technology, Xuzhou, China, 2013. Available online: http://cdmd.cnki.com.cn/Article/CDMD-10290-1013030104.htm (accessed on 1 May 2013).
51. Ren, J.; Tamaki, K.; Li, S.; Junxia, Z. Late Mesozoic and Cenozoic rifting and its dynamic setting in Eastern China and adjacent areas. *Tectonophysics* **2002**, *344*, 175–205. [CrossRef]
52. Deng, J.; Hou, Z.; Mo, X.; Yang, L.; Wang, Q.; Wang, C. Superimposed orogenesis and metallogenesis in Sanjiang Tethys. *Miner. Depos.* **2010**, *29*, 37–42. (In Chinese with English Abstract). [CrossRef]
53. Teng, J. *Coal Structure Prediction Based on Geophysical Logging*; China University of Geosciences: Beijing, China, 2016. Available online: https://kns.cnki.net/kcms2/article/abstract?v=6uDTENTNErAlc3LIlE2xHBcpHKMdHdh0viODqUpf8swyjzygZLB0MUwVCCMiPy4DOJpBsi2Si51pfl-jY9ua7rLhpASAJz2S4AVCVZZ2DLCA2V60zJUWh69USBr1N9eE&uniplatform=NZKPT&language=CHS (accessed on 7 December 2016).
54. Li, Y.; Zhang, Y.; Zhang, L.; Hou, J. Characterization on pore structure of tectonic coals based on the method of mercury intrusion, carbon dioside adsorption and nitrogen adsorption. *J. China Coal Soc.* **2019**, *44*, 1188–1196. [CrossRef]